

EvoEye: Self-Evolving Runtime Monitoring for Autonomous Driving Systems

Mingfei Cheng, Lionel Briand, *Fellow, IEEE*, and Xiaofei Xie

Abstract—Runtime monitoring is essential for detecting impending hazards in autonomous driving systems (ADSs). However, existing ADS runtime monitors have fixed detection capabilities: rule-based monitors cover only manually specified hazards, while learning-based monitors depend heavily on their initial training data and may retain substantial prediction errors. We therefore propose *EvoEye*, which identifies the current monitor’s errors, generates informative executions accordingly, and updates the monitor through self-evolution. To enable effective self-evolution, *EvoEye* combines a capable runtime monitor with targeted scenario acquisition. *FusionMonitor* learns cross-module temporal interactions for collision prediction, while *BlindSpotEvolver* converts current prediction errors into search guidance and uses density-aware mutation to acquire informative executions for subsequent monitor updates.

We evaluate *EvoEye* on Baidu Apollo with CARLA in representative highway and urban scenarios. *FusionMonitor* improves frame-level Recall by up to 37.8 percentage points at a false positive rate of 0.05, with 2.49 ms latency and 2.8–4.2 seconds of median warning time. Under the same budget, *BlindSpotEvolver* outperforms uniform and violation-oriented sampling by up to 13.2 F1 points on previously missed unsafe contexts.

I. INTRODUCTION

Autonomous driving systems (ADSs) have advanced rapidly in recent years and offer the potential to improve transportation safety, accessibility, and efficiency [1]. An ADS comprises the hardware and software that collectively perform the dynamic driving task on a sustained basis. In a typical modular architecture, observations from cameras, LiDAR, radar, and positioning sensors are processed to perceive and understand the surrounding environment; the resulting information is then used for behavior prediction, decision-making, motion planning, and vehicle control [2]. Despite substantial progress, assuring the safety of ADSs remains challenging because they operate in open and highly dynamic environments and rely on complex, partly learning-enabled components whose behaviors cannot be exhaustively validated before deployment [3], [4]. Runtime monitoring therefore serves as an important complementary safeguard by continuously assessing ADS executions and detecting emerging hazards that escape design-time assurance [5].

Existing runtime monitoring approaches for ADSs broadly rely on either rule-based safety indicators or learning-based misbehavior predictors. Rule-based approaches use predefined indicators, such as Time-to-Collision (TTC) [6] and

Responsibility-Sensitive Safety (RSS) [7], to determine whether current vehicle interactions violate specific safety conditions. Although efficient and interpretable, these indicators are typically designed for particular conflict patterns and rely on a limited set of kinematic relationships, making it difficult to characterize compound traffic interactions and failures emerging across the full ADS stack. Learning-based monitors [8], [9] provide greater expressive power by learning complex temporal patterns directly from execution data, rather than relying on manually specified safety rules. This enables them to integrate high-dimensional runtime signals and identify risk patterns that may not be captured by individual safety indicators. However, existing approaches typically infer impending failures from sensor observations or model-local signals, such as reconstruction errors and neural activation patterns. Such signals provide only a partial view of a full-stack ADS, which combines learning-based perception and prediction with logic- and optimization-driven planning and control [10]. Safety violations may arise from inconsistencies and error propagation across these interacting modules, even when no individual input or model appears anomalous. Moreover, existing monitors are typically developed once on a fixed dataset, which limits their capability to the behaviors covered during training. Given the vast execution space of an ADS, the initial dataset may leave important monitoring blind spots. This motivates a monitor that can actively collect informative executions and iteratively improve its monitoring capability.

To bridge this gap, we investigate self-evolving runtime monitoring, in which the monitor closes the loop between monitoring feedback, targeted execution collection, and iterative model updates to progressively improve its capability. However, realizing such a monitor presents two main challenges. First, the monitor must remain discriminative as evolution introduces increasingly difficult and diverse executions. Distinguishing subtle pre-crash patterns from complex yet safe behaviors requires a system-level representation that captures temporal dependencies and cross-module interactions across the full ADS stack. Therefore, designing a monitor with sufficient expressive capacity to learn from progressively harder execution data remains challenging. Second, self-evolution must be data-efficient under a limited simulation budget. The high-dimensional scenario space makes exhaustive exploration infeasible. Uniform sampling may waste substantial effort on less informative executions, whereas violation-oriented fuzzing may repeatedly exploit known collision-prone regions without addressing the monitor’s remaining weaknesses. Therefore, effectively prioritizing executions that expose current monitor-

Mingfei Cheng and Xiaofei Xie are with the School of Computing and Information Systems, Singapore Management University, Singapore. (E-mail: mfcheng.2022@smu.edu.sg, xfxie@smu.edu.sg).

Lionel Briand is with the University of Ottawa, Canada, and Lero Research Ireland Centre for Software Research, University of Limerick, Ireland. (E-mail: lbriand@uottawa.ca)

ing blind spots and provide the greatest value for subsequent updates remains challenging.

To address these challenges, we propose *EvoEye*, a self-evolving runtime monitoring framework for full-stack ADSs. *EvoEye* consists of two tightly coupled components, *FusionMonitor* and *BlindSpotEvolver*, which respectively determine how to characterize system-level risks and how to acquire the execution evidence needed to improve their detection. To tackle the first challenge, we design *FusionMonitor*, a learning-based monitor that jointly models temporal dependencies and cross-module interactions among runtime messages from perception, prediction, planning, and control. Its learning-based design enables iterative updates with newly acquired execution data, progressively improving the distinction between emerging collision risks and complex yet safe behaviors. Building on the *FusionMonitor*, *BlindSpotEvolver* addresses the second challenge by using its prediction errors to guide subsequent data acquisition. Rather than searching only for collisions, it prioritizes executions that expose current monitoring weaknesses, while a density-aware mechanism avoids repeatedly exploring well-sampled regions. The acquired executions update the monitor, which then guides the next evolution round, forming a closed self-evolution loop that progressively improves monitoring performance.

We evaluate *EvoEye* on Baidu Apollo [10] with CARLA [11] in representative highway and urban scenarios. At a target FPR of 0.05, *FusionMonitor* improves frame-level Recall over the strongest baseline by 37.8 and 29.8 percentage points, while incurring only 2.49 ms of CPU latency and providing median warning times of 4.2 and 2.8 seconds. Under the same evolution budget, *BlindSpotEvolver* outperforms uniform sampling and violation-oriented fuzzing by up to 13.2 F1 points, demonstrating the effectiveness and practicality of *EvoEye*.

In summary, this paper makes the following contributions:

- To the best of our knowledge, we propose the first self-evolving runtime monitoring framework for full-stack ADSs.
- We design *FusionMonitor*, which jointly models temporal dependencies and cross-module interactions in ADS runtime signals for collision-risk prediction.
- We design *BlindSpotEvolver*, which uses monitor prediction errors and density-aware sampling to acquire informative executions and iteratively update the monitor.
- We evaluate *EvoEye* on the industrial-grade Baidu Apollo ADS with CARLA, demonstrating effective runtime monitoring and consistent gains from self-evolution.

II. BACKGROUND AND FORMULATION

A. Autonomous Driving Systems

Autonomous driving systems (ADSs) are the core intelligence of autonomous vehicles (AVs), enabling vehicles to perceive the environment and make driving decisions with limited or no human intervention. Existing ADSs can generally be categorized into two major paradigms: *module-based* ADSs and *end-to-end (E2E)* ADSs. *Module-based* ADSs, such as Pylot [12], Baidu Apollo [10], and Autoware [13],

are widely adopted in industrial and research settings due to their interpretable and well-structured designs. A module-based ADS is typically decomposed into several functional components, including *Localization*, *Perception*, *Prediction*, *Planning*, and *Control*. The localization module estimates the ego vehicle’s pose by fusing information from sensors such as GPS, IMU, and LiDAR. The perception module processes multimodal sensor inputs, such as camera images, LiDAR point clouds, and radar signals, to detect and track surrounding traffic participants. The prediction module estimates the future behaviors or trajectories of nearby actors, while the planning module generates a feasible trajectory for the ego vehicle. Finally, the control module translates the planned trajectory into low-level actuation commands, such as steering, throttle, and braking. In contrast, *end-to-end ADSs* have recently attracted increasing attention with the rapid development of deep learning techniques. Instead of explicitly decomposing the driving task into multiple functional modules, E2E approaches [14]–[19] directly map sensor observations to driving actions or future trajectories through a unified model.

In this paper, we monitor ADS using observable runtime signals within the system. For example, these signals are obtained from inter-module messages, such as perception outputs, predicted trajectories, planning, and control commands.

B. Scenario

Scenarios provide a fundamental abstraction for testing ADSs within their Operational Design Domain (ODD), which specifies the environmental, roadway, traffic, and operational conditions under which an ADS is intended to operate [20]. Following established terminology [21], scenarios can be described at three levels of abstraction. A *functional scenario* provides a high-level description of the road layout, traffic participants, and their interactions. A *logical scenario* refines this description by defining configurable parameters, together with their ranges and constraints. A *concrete scenario* assigns a specific value to each parameter, yielding an executable test case. Because the operational space of an ADS is too large to enumerate exhaustively, logical scenarios are commonly used to define manageable yet diverse spaces of concrete executions [22]–[25]. In this paper, we use logical scenarios as the parameterized spaces from which runtime executions are generated for monitor training and self-evolution. For example, an unprotected intersection logical scenario specifies configurable properties such as vehicle initial positions, speeds, and activation times. Assigning values to these parameters produces a concrete scenario, whose execution provides the runtime observations used by the monitor.

Formally, we denote the logical scenario space by \mathcal{X} , where each point $x \in \mathcal{X}$ represents a concrete scenario instantiated by a specific assignment of scenario parameters. Given an ADS under test $\mathcal{A} = \{m_1, \dots, m_K\}$, executing a scenario x in simulation produces two types of observations:

$$\mathbf{O}(x), \mathbf{M}(x) = f_{\text{sim}}(x, \mathcal{A}), \quad (1)$$

where f_{sim} denotes the simulation procedure. Here, $\mathbf{O}(x)$ denotes the *scenario observation* obtained from the simulator, while $\mathbf{M}(x)$ denotes the *runtime observation* collected from the internal execution of the ADS.

The *scenario observation* is defined as $\mathbf{O}(x) = (\mathbf{o}_1, \dots, \mathbf{o}_T)$, where \mathbf{o}_t describes the external scene state at time step t . Specifically, $\mathbf{o}_t = \{y_t^i | i \in \mathbb{P}\}$, where \mathbb{P} denotes the set of traffic actors, including the ego vehicle, NPC vehicles, and pedestrians. For each actor i , its state is defined as $y_t^i = \{p_t^i, \theta_t^i, v_t^i, a_t^i\}$, where p_t^i , θ_t^i , v_t^i , and a_t^i denote its center position, heading angle, velocity, and acceleration at time step t , respectively. Unless otherwise specified, we use $i = 0$ to denote the ego vehicle controlled by the ADS \mathcal{A} .

The *runtime observation* captures ADS-internal observable information produced during execution. We denote the runtime observation sequence of scenario x as $\mathbf{M}(x) = (\mathbf{m}_1, \dots, \mathbf{m}_T)$, where each $\mathbf{m}_t = (\mathbf{m}_t^1, \mathbf{m}_t^2, \dots, \mathbf{m}_t^K)$ contains the runtime information emitted by the ADS modules at time step t . Here, \mathbf{m}_t^k denotes the internal observation associated with module m_k , such as intermediate outputs generated by perception, prediction, planning, and control modules. Thus, $\mathbf{O}(x)$ provides simulator-level scene information, whereas $\mathbf{M}(x)$ provides ADS-internal runtime observable information used to characterize the system's runtime behavior. For convenience, we define the *Scenario Record* of a scenario x as $D(x) = (x, \mathbf{M}(x), \mathbf{O}(x))$, which includes its complete execution result.

III. PROBLEM DEFINITION

Given the internal runtime signals observable from an ADS, our goal is to predict whether its current execution will result in a collision within a future time horizon. We focus on collisions as the target safety violation because they represent a critical safety outcome for autonomous driving systems [23], [25], [26]. Beyond runtime prediction, we aim to enable the monitor to iteratively improve its effectiveness by using monitoring feedback to guide the acquisition of new execution data. We next formalize the runtime monitoring task and define the self-evolving runtime monitoring problem.

Definition 1 (Violation Scenario and Frame Label). *Given a concrete scenario $x \in \mathcal{X}$, executing the ADS \mathcal{A} in x produces a scenario observation $\mathbf{O}(x) = (\mathbf{o}_1, \dots, \mathbf{o}_T)$. Let $\nu(\mathbf{o}_t) \in \{0, 1\}$ indicate whether the ego vehicle is involved in a collision at frame t . The collision frame is defined as $t_{\text{col}}(x) = \min\{t | \nu(\mathbf{o}_t) = 1\}$, where $t_{\text{col}}(x) = +\infty$ if no collision occurs during the execution. A scenario x is a violation scenario if $t_{\text{col}}(x) < +\infty$.*

Let τ_t denote the timestamp of frame t , and let $\tau_{\text{col}}(x) = \tau_{t_{\text{col}}(x)}$ denote the collision timestamp. Given a prediction horizon H , the label of frame t is defined as

$$y_t(x) = \mathbb{1}[0 < \tau_{\text{col}}(x) - \tau_t \leq H], \quad (2)$$

where $\mathbb{1}[\cdot]$ is the indicator function. Therefore, $y_t(x) = 1$ indicates that a collision will occur within the next H seconds, whereas $y_t(x) = 0$ otherwise.

Note that the scenario observation $\mathbf{O}(x)$ is used only to derive the ground-truth labels; the runtime monitor does not access this privileged information during prediction.

Definition 2 (Runtime Monitor). *At frame t , the runtime context of length L is defined as $\mathbf{c}_t = (\mathbf{m}_{\max(1, t-L+1)}, \dots, \mathbf{m}_t)$, where $\mathbf{m}_t = (\mathbf{m}_t^1, \dots, \mathbf{m}_t^K)$ contains the runtime signals observable from the K ADS modules at frame t . A runtime monitor \mathcal{G} maps the current runtime context to a collision-risk score $\mathcal{G}(\mathbf{c}_t) \in [0, 1]$. The score estimates the risk that the ongoing execution will result in a collision within the next H seconds, with a higher score indicating greater predicted risk.*

The objective of runtime monitoring is to distinguish runtime contexts that precede an imminent collision from those that do not. However, a monitor trained on a fixed set of executions may remain unreliable for runtime behaviors that are underrepresented in its training data. Conventional retraining is typically open loop, as additional executions are collected without considering the monitor's current capability and may therefore fail to address its remaining weaknesses.

Self-evolving runtime monitoring closes this loop by allowing the current monitor to guide the acquisition of new scenario records. The acquired records are used to update the monitor, which subsequently guides the next acquisition round. This iterative process enables data acquisition to adapt to the evolving monitoring capability, which is formally defined as:

Definition 3 (Self-Evolving Runtime Monitoring). *Let \mathcal{G}_r and \mathcal{D}_r denote the runtime monitor and the accumulated scenario records at evolution round r , respectively. Given an evolution budget B_r , self-evolving runtime monitoring iteratively acquires new records using the current monitor:*

$$\mathcal{D}'_r = \pi(\mathcal{X}, \mathcal{G}_r, \mathcal{D}_r; B_r), \quad (3)$$

where π is a monitor-guided acquisition strategy. The acquired records are added to the accumulated record set, and the monitor is updated accordingly:

$$\mathcal{D}_{r+1} = \mathcal{D}_r \cup \mathcal{D}'_r, \quad \mathcal{G}_{r+1} = \text{Update}(\mathcal{G}_r, \mathcal{D}_{r+1}). \quad (4)$$

Research Goal. The self-evolving runtime monitoring forming a closed loop between scenario record acquisition and monitor improvement. The overall research goal is to maximize the monitoring effectiveness of the evolved monitor within a limited simulation-time budget. Formally, given an ADS \mathcal{A} , a logical scenario space \mathcal{X} , an initial set of scenario records \mathcal{D}_0 , and a total simulation-time budget B , our goal is to obtain a runtime monitor \mathcal{G}_R with high monitoring effectiveness after R rounds of self-evolution. We formulate this objective as

$$\begin{aligned} & \text{maximize} && \mathbb{E}_{(\mathbf{c}, y) \sim \mathcal{P}_{\mathcal{C}}} [f_{\text{eval}}(\mathcal{G}_R(\mathbf{c}), y)] \\ & \text{subject to} && \sum_{r=0}^{R-1} \text{cost}(\mathcal{D}'_r) \leq B, \end{aligned} \quad (5)$$

where $\mathcal{P}_{\mathcal{C}}$ denotes the distribution of labeled runtime contexts induced by the ADS \mathcal{A} and the logical scenario space \mathcal{X} , and f_{eval} measures the quality of the predicted collision-risk score with respect to the ground-truth label. Moreover,

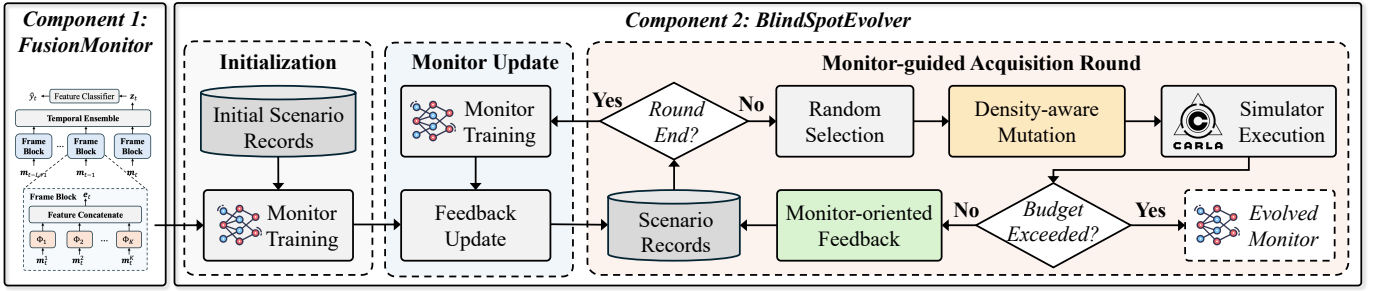


Fig. 1: Overview of *EvoEye*.

$\text{cost}(\mathcal{D}'_r)$ denotes the simulation time required to acquire the new scenario records \mathcal{D}'_r at evolution round r . Achieving this goal requires addressing two closely coupled subproblems. First, the runtime monitor must have sufficient representational and learning capacity to capture the complex temporal and cross-module dependencies among heterogeneous ADS runtime signals. This capability is a prerequisite for self-evolution: a monitor with limited capacity, such as a fixed rule-based monitor, cannot substantially improve merely by acquiring additional scenario execution records. Achieving this goal requires addressing two closely coupled subproblems. Second, the acquisition strategy π should translate feedback from the current monitor into effective guidance for searching the large scenario space. It should prioritize scenarios that expose the monitor's current weaknesses and yield informative scenario records, thereby efficiently improving the monitor within the available simulation-time budget.

IV. METHODOLOGY

A. Overview

Figure 1 presents an overview of *EvoEye*, which consists of two components: *FusionMonitor* and *BlindSpotEvolver*. *FusionMonitor* provides a learning-based runtime monitor that models heterogeneous and temporally dependent ADS runtime signals to predict impending collisions. *BlindSpotEvolver* iteratively improves the monitor through two mechanisms, *Monitor-oriented Feedback* and *Density-aware Mutation*, which jointly guide the acquisition of informative scenario records.

FusionMonitor. As shown in Fig. 2, *FusionMonitor* fuses runtime signals from multiple ADS modules at each frame and models their temporal dependencies over the runtime context. It then outputs a collision-risk score for the prediction horizon. Its learning-based design enables continuous updates as new scenario records become available.

BlindSpotEvolver. This component iteratively evolves the monitor through multiple monitor-guided acquisition rounds. It first trains an initial monitor using the initial scenario records. In each subsequent round, it derives feedback from the current monitor to guide the acquisition of informative scenarios from the logical scenario space. The resulting scenario records are added to the accumulated record set and used to update the monitor. The updated monitor then provides new feedback for the next acquisition round, forming a closed loop between scenario acquisition and monitor improvement. This

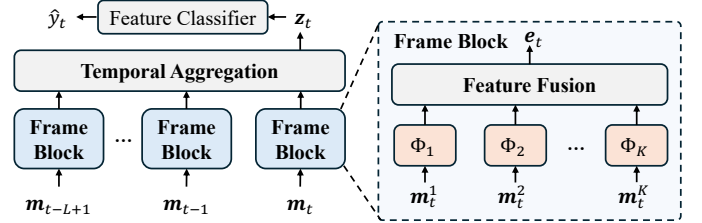


Fig. 2: Architecture of *FusionMonitor*.

Table I: Module-specific encoders used by *FusionMonitor*.

Module	Input Description	Encoder Structure
Perception	States of detected obstacles	$\{\hat{\mathbf{o}}_{t,i}\}_{i=1}^{n_t} \xrightarrow{\text{Shared MLP} + \text{AttnPool}} \mathbf{z}_t^{\text{perc}}$
Prediction	Predicted trajectories of obstacles	$\{\mathbf{p}_{t,i}\}_{i=1}^{n_t} \xrightarrow{\text{Shared MLP} + \text{AttnPool}} \mathbf{z}_t^{\text{pred}}$
Planning	Planned ego trajectory	$\mathbf{P}_t \xrightarrow{\text{Flatten} + \text{MLP}} \mathbf{z}_t^{\text{plan}}$
Control	Action commands	$\mathbf{u}_t \xrightarrow{\text{MLP}} \mathbf{z}_t^{\text{ctrl}}$

process continues until the simulation-time budget is exhausted, producing the final evolved monitor.

B. Runtime Monitor: *FusionMonitor*

As discussed in Section III, effective self-evolution requires a runtime monitor with sufficient capacity to learn from increasingly diverse and challenging scenario executions. Otherwise, acquiring additional execution records may yield limited improvement in monitoring capability. Designing such a monitor is challenging because runtime signals from different ADS modules vary substantially in structure and semantics, while impending collisions often emerge from their interactions over multiple frames rather than from any individual frame.

To address these challenges, we design *FusionMonitor* with a hierarchical feature-fusion architecture, as illustrated in Fig. 2. At each frame, a *Frame Block* encodes the heterogeneous module-level signals and fuses them into a unified frame feature. The *Temporal Aggregation* then aggregates the representations of the latest L frames to capture their temporal dependencies. Finally, a classifier maps the aggregated feature to a collision-risk score indicating whether the current execution will result in a collision within the next H seconds. We detail the main components of *FusionMonitor* below.

Frame Block. Formally, given a runtime observation $\mathbf{m}_t = (\mathbf{m}_t^1, \mathbf{m}_t^2, \dots, \mathbf{m}_t^K)$ at time step t , where \mathbf{m}_t^k denotes the message emitted by the k -th ADS module, we apply a module-

specific encoder $\Phi_k(\cdot)$ to encode key attributes from \mathbf{m}_t^k and convert them into a fixed-length feature $\mathbf{z}_t^k = \Phi_k(\mathbf{m}_t^k) \in \mathbb{R}^{d_k}$. Table I summarizes the module-specific encoders used by *FusionMonitor* for module-based ADSs. Perception and prediction signals are encoded from variable-sized sets of surrounding obstacles using shared MLPs and attention pooling. Planning trajectories are flattened and encoded by an MLP, while control commands are directly mapped to a fixed-length representation through an MLP.

We concatenate the module-level representations and apply a frame-level MLP with nonlinear activations to obtain a unified frame representation:

$$\mathbf{z}_t = \text{MLP}_{\text{frame}}(\text{Concat}(\mathbf{z}_t^1, \dots, \mathbf{z}_t^K)). \quad (6)$$

This representation captures nonlinear interactions among the runtime signals from different ADS modules at time step t .

Temporal Aggregation. Since driving decisions depend on recent execution history, *FusionMonitor* aggregates the frame representations within a context window of length L . We adopt simple concatenation to preserve the information and temporal order of all frames while keeping the model lightweight. For a runtime context $\mathbf{c}_t = (\mathbf{m}_{t-L+1}, \dots, \mathbf{m}_t)$, we first concatenate the corresponding frame-level feature in temporal order. We then apply an MLP with nonlinear activation functions to capture interactions across frames and obtain a compact temporal feature:

$$\mathbf{h}_t = \text{MLP}_{\text{temp}}(\text{Concat}(\mathbf{z}_{t-L+1}, \dots, \mathbf{z}_t)), \quad (7)$$

where MLP_{temp} consists of fully connected layers with ReLU activations. The resulting representation \mathbf{h}_t captures the joint evolution of the runtime signals over the latest L frames.

Feature Classifier. The encoded feature \mathbf{h}_t is fed into a fully connected classifier to predict a collision-risk score:

$$\hat{y}_t = \mathcal{G}(\mathbf{c}_t) = \sigma(f_{\text{cls}}(\mathbf{h}_t)), \quad (8)$$

where $\sigma(\cdot)$ is the sigmoid function. The output $\hat{y}_t \in [0, 1]$ indicates the risk that a collision will occur within the next H seconds, with a higher score indicating higher collision risk.

Monitor Training. Given a set of scenario records \mathcal{D} , we extract a labeled runtime-context dataset $\mathcal{T} = \{(\mathbf{c}_j, y_j)\}$, where $y_j \in \{0, 1\}$ indicates whether a collision will occur within the prediction horizon H . The *FusionMonitor* is then trained by minimizing the binary cross-entropy loss:

$$\mathcal{G}^* = \arg \min_{\mathcal{G}} \frac{1}{|\mathcal{T}|} \sum_{(\mathbf{c}_j, y_j) \in \mathcal{T}} \ell_{\text{BCE}}(\mathcal{G}(\mathbf{c}_j), y_j). \quad (9)$$

C. Self-Evolution Loop: *BlindSpotEvolver*

The goal of self-evolution is to discover scenarios whose executions expose blind spots of the current monitor and provide informative scenario records for its improvement. This is challenging because the logical scenario space is vast. Naive strategies such as random sampling may therefore consume substantial simulation time on low-value executions that provide little useful information for improving the monitor.

To address this problem, *EvoEye* introduces *BlindSpotEvolver*, a search-based self-evolution pipeline, as illustrated

in Fig. 1. *BlindSpotEvolver* first trains an initial monitor using the available initial scenario records. It then iteratively acquires new scenario records to improve the current monitor. At each iteration, it randomly selects a previously executed scenario as the seed and applies *Density-Aware Mutation* to generate a new scenario, and executes it in the simulator. The resulting scenario record is evaluated by *Monitor-Oriented Feedback* to calculate its feedback and then added to the accumulated scenario record set. At the end of each evolution round, defined by the acquisition of a fixed number of new scenario records, *BlindSpotEvolver* updates the monitor using the expanded record set and recomputes the feedback for all previously executed scenarios. The updated monitor and feedback then guide the next acquisition round. This closed-loop process continues until the simulation-time budget is exhausted, yielding the final evolved monitor.

1) *Feedback Calculation:* *BlindSpotEvolver* prioritizes scenarios that expose weaknesses of the current monitor. Conventional safety metrics, such as minimum distance, measure execution criticality but do not directly reflect monitoring errors. We therefore define *Monitor-Oriented Feedback* based on the prediction error of the current monitor. Formally, for an executed scenario x , let $\mathcal{C}(x) = (\mathbf{c}_1, \dots, \mathbf{c}_{n_x})$ denote its runtime contexts. At evolution round r , the monitor outputs $\hat{y}_i^{(r)} = \mathcal{G}_r(\mathbf{c}_i)$ for each context \mathbf{c}_i , with ground-truth label $y_i \in \{0, 1\}$. We define the scenario-level feedback as the average prediction error:

$$f_r(x) = \frac{1}{n_x} \sum_{i=1}^{n_x} |\hat{y}_i^{(r)} - y_i|. \quad (10)$$

A larger $f_r(x)$ indicates that the current monitor performs less accurately on scenario x . Whenever the monitor is updated, the feedback scores of all scenario records are recomputed.

2) *Density-Aware Mutation:* In each iteration, *BlindSpotEvolver* generates a new scenario by mutating a previously executed scenario. However, repeated local mutation may waste the simulation budget when the neighborhood of a seed has already been sufficiently explored, whereas relying only on global sampling may overlook underexplored local regions that could provide useful data for monitor improvement.

To balance local exploitation and global exploration, we design *Density-Aware Mutation*, which evaluates the potential of the region around the selected seed. Regions with high potential are exploited locally, whereas regions with low potential favor global exploration.

Region Exploit Potential. Given a selected seed scenario x from \mathcal{D} , we define the neighborhood of x in the logical scenario space as

$$\mathcal{N}_\delta(x) = \{x' \in \mathcal{X} \mid d_{\mathcal{X}}(x', x) \leq \delta\}, \quad (11)$$

where $d_{\mathcal{X}}(\cdot, \cdot)$ measures the distance between two scenarios and δ is the neighborhood radius. The previously executed scenarios within this neighborhood are denoted as $\mathcal{S}_\delta(x)$.

We then characterize the potential of the neighborhood using the mean and standard deviation of its normalized monitor-oriented feedback:

$$\begin{aligned}\mu_\delta(x) &= \frac{1}{|\mathcal{S}_\delta(x)|} \sum_{x_j \in \mathcal{S}_\delta(x)} \bar{f}_r(x_j), \\ \sigma_\delta(x) &= \sqrt{\frac{1}{|\mathcal{S}_\delta(x)|} \sum_{x_j \in \mathcal{S}_\delta(x)} (\bar{f}_r(x_j) - \mu_\delta(x))^2},\end{aligned}\quad (12)$$

where $\bar{f}_r(x_j)$ denotes the normalized feedback of scenario x_j . A high $\mu_\delta(x)$ indicates that the neighborhood consistently exposes limitations of the current monitor. A high $\sigma_\delta(x)$ indicates substantial feedback variation among nearby scenarios, suggesting that small scenario changes may reveal different monitoring behaviors and additional blind spots. We therefore define the regional exploit potential as

$$q_\delta(x) = \mu_\delta(x) + \sigma_\delta(x). \quad (13)$$

Mutation Strategy. Based on the regional exploit potential, we determine whether to explore the neighborhood of the selected seed or the global scenario space. We first normalize the regional potential across all previously executed scenarios:

$$p_\delta(x) = \frac{q_\delta(x) + \epsilon}{\max_{x_j \in \mathcal{D}} q_\delta(x_j) + \epsilon}, \quad (14)$$

where ϵ is a small constant that prevents division by zero. Then, the mutation generates a new scenario x' through either local mutation or global exploration:

$$x' \sim \begin{cases} \text{UniformSample}(\mathcal{N}_\delta(x)), & \text{if } \xi < p_\delta(x), \\ \text{UniformSample}(\mathcal{X}), & \text{otherwise,} \end{cases} \quad (15)$$

where $\xi \sim \text{Uniform}(0, 1)$. Thus, a region with high exploit potential is more likely to be mutated locally, whereas global exploration is favored when the region has low exploit potential.

D. Algorithm Overview

Algorithm 1 summarizes the overall workflow of *BlindSpotEvolver* in *EvoEye*. Given the logical scenario space \mathcal{X} , the target ADS \mathcal{A} , and the initial scenario records $\mathcal{D}_{\text{init}}$, *BlindSpotEvolver* iteratively acquires new records and updates the monitor until the simulation-time budget is exhausted, producing an evolved runtime monitor. *BlindSpotEvolver* first trains the initial monitor \mathcal{G}_0 using $\mathcal{D}_{\text{init}}$ (Line 1). It then computes the monitor-oriented feedback of each initial record using \mathcal{G}_0 , forming the initial record set \mathcal{D}_0 (Line 2). The feedback calculation is detailed in Section IV-C1. Within the simulation-time budget, *BlindSpotEvolver* repeatedly acquires new scenario records to improve the monitor (Lines 4–14). At each iteration, *Density-Aware Mutation* randomly selects a seed from the current record set \mathcal{D}_r and generates a new scenario x through local mutation or global sampling (Lines 6–7). This process is detailed in Section IV-C2. The generated scenario is executed with \mathcal{A} , producing the internal runtime signals $\mathbf{M}(x)$ and scenario observations $\mathbf{O}(x)$ (Line 8). *BlindSpotEvolver* then calculates its feedback score $f_r(x)$ using the current monitor \mathcal{G}_r and

Algorithm 1: Self-evolution procedure of *EvoEye*.

```

Input      : Scenario space  $\mathcal{X}$ , target ADS  $\mathcal{A}$ , initial
              scenario records  $\mathcal{D}_{\text{init}}$ 
Output    : Evolved runtime monitor  $\mathcal{G}_r$ 
Parameters: Evolution time budget  $T_{\text{budget}}$ , evolution round
              budget  $N_{\text{round}}$ 

//Train the initial monitor
1  $\mathcal{G}_0 \leftarrow \text{MonitorUpdate}(\text{None}, \mathcal{D}_{\text{init}})$ 
//Initialize scenario feedback
2  $\mathcal{D}_0 \leftarrow \text{FeedbackRefresh}(\mathcal{D}_{\text{init}}, \mathcal{G}_0)$ 
3  $r \leftarrow 0, i \leftarrow 0, t_{\text{start}} \leftarrow \text{CURRENTTIME}()$ 
4 while  $\text{CURRENTTIME}() - t_{\text{start}} < T_{\text{budget}}$  do
5    $i \leftarrow i + 1$ 
6    $x' \leftarrow \text{RANDOMSELECT}(\mathcal{D}_r)$ 
7    $x \leftarrow \text{DensityAwareMutation}(x', \mathcal{X}, \mathcal{D}_r)$ 
8    $\mathbf{O}(x), \mathbf{M}(x) \leftarrow \text{SIMULATION}(x, \mathcal{A})$ 
9    $f_r(x) \leftarrow \text{MonitorFeedback}(\mathbf{O}(x), \mathbf{M}(x), \mathcal{G}_r)$ 
10   $\mathcal{D}_r \leftarrow \mathcal{D}_r \cup \{(x, \mathbf{O}(x), \mathbf{M}(x), f_r(x))\}$ 
11  if  $i \bmod N_{\text{round}} = 0$  then
12     $\mathcal{G}_{r+1} \leftarrow \text{MonitorUpdate}(\mathcal{G}_r, \mathcal{D}_r)$ 
13     $\mathcal{D}_{r+1} \leftarrow \text{FeedbackRefresh}(\mathcal{D}_r, \mathcal{G}_{r+1})$ 
14     $r \leftarrow r + 1$ 
15 return  $\mathcal{G}_r$ 

```

adds the resulting scenario record to \mathcal{D}_r (Lines 9–10). After every N_{round} iterations, *BlindSpotEvolver* updates the monitor using the expanded record set, producing \mathcal{G}_{r+1} (Line 12). Because the feedback scores depend on the current monitor, *BlindSpotEvolver* subsequently recomputes the feedback of all accumulated records using \mathcal{G}_{r+1} (Line 13). The updated monitor and record set are then used in the next evolution round. This process continues until the simulation-time budget T_{budget} is exhausted, after which *BlindSpotEvolver* returns the latest runtime monitor \mathcal{G}_r (Line 15).

V. EMPIRICAL EVALUATION

In this section, we empirically evaluate *EvoEye* by answering the following research questions:

RQ1 (Monitoring Effectiveness). How effectively does *EvoEye* detect impending safety violations compared with existing runtime monitoring approaches?

RQ2 (Self-Evolution Effectiveness). To what extent does self-evolution improve the monitoring effectiveness of *EvoEye*, and how efficiently does it acquire useful runtime evidence compared with alternative scenario-sampling strategies under the same evolution budget?

RQ3 (Component Contributions). How does each component of *EvoEye* contribute to its monitoring and self-evolution?

Environment. We conduct our experiments on *Apollo* [10], an open-source, industrial-grade, full-stack autonomous driving system developed by Baidu [10]. We select *Apollo* because it provides a complete and modular autonomy stack, covering perception, prediction, planning, and control, and has been widely adopted in ADS research and evaluation [25], [27]. We integrate *Apollo* with the CARLA simulator and enable its native sensor-processing and decision-making pipeline. Specifically, *Apollo* receives raw observations from simulated onboard sensors and

Table II: Dataset statistics. #Scena.-the number of scenarios; #Viol.-the number of collision scenarios; #Frames-the number of frames; #Unsafe-the number of frames labeled as unsafe.

LS	Set	#Scena.	#Viol. (%)	#Frame	#Unsafe (%)
S1	Train	107	36 (33.6%)	43,128	1,778 (4.1%)
	Val	25	6 (24.0%)	10,330	301 (2.9%)
	Test	75	25 (33.3%)	32,546	1,242 (3.8%)
S2	Train	177	137 (77.4%)	38,321	6,355 (16.6%)
	Val	45	35 (77.8%)	9,639	1,637 (17.0%)
	Test	132	99 (75.0%)	29,783	4,551 (15.3%)

processes them through its perception, prediction, planning, and control modules. This setup differs from prior ADS testing studies that bypass the perception stack [25], [27] by directly providing ground-truth environmental information from the simulator to the ADS. By retaining the complete perception-to-control pipeline, our environment preserves perception errors, thereby providing a more realistic setting for evaluating runtime monitoring of full-stack ADS executions.

Logical Scenarios. We evaluate *EvoEye* on two safety-critical logical scenarios derived from the NHTSA pre-crash typology [28]: (1) *S1: highway cut-in* and (2) *S2: unprotected intersection*. They represent common highway and urban driving conditions and involve multiple interacting maneuvers. *S1: Highway cut-in*. The ego vehicle interacts with six vehicles in a multi-lane highway scenario involving car following, overtaking, cut-ins from adjacent lanes, and sudden lead-vehicle braking. We expose 20 parameters controlling vehicle positions, speeds, cut-in triggers, and braking behaviors. *S2: Unprotected intersection*. The ego vehicle proceeds through a four-way intersection while interacting with five vehicles performing opposing turns, lateral crossings, and right-turn merging. We expose 10 parameters controlling their speeds and start times.

Baselines. We organize the baselines into two groups corresponding to the two key capabilities of *EvoEye*: runtime monitoring and self-evolution. (1) *Runtime monitoring (RQ1)*. We compare *EvoEye* against two rule-based safety indicators and one learning-based baseline. The safety indicators include *TTC* (time to collision) [6] and *RSS* (Responsibility-Sensitive Safety) [7]. We further implement *AutoEncode-Monitor (AEM)*, a reconstruction-based anomaly detector inspired by SelfOracle [8]. Unlike SelfOracle, which operates on sensor observations, *AEM* takes the same module-internal messages as *EvoEye* as input. It is trained on collision-free frames and uses reconstruction error as the runtime anomaly score. (2) *Self-Evolution (RQ2)*. We compare the self-evolution strategy of *EvoEye* against three baselines. *EvoEye** performs no further evolution after initial training. *Uniform* randomly samples configurations from the logical-scenario parameter space. *AVFuzzer* [23] applies a genetic algorithm to search for safety-critical scenarios.

Datasets. To evaluate the runtime monitors and initialize self-evolution, we use uniform sampling to collect execution data for 12 hours for each logical scenario (LS). The data collected during the first 6 hours are used as the training set and the initial dataset for self-evolution. The data collected during the

remaining 6 hours are held out and split into a validation set and a test set at a 1:3 ratio. Each frame at time t is labeled according to whether a collision occurs within the following $H = 3$ seconds. We set $H = 3$ seconds based on prior studies that consider 0.5–3 seconds before impact an effective interval for preventive intervention [9], [29], [30]. We adopt the upper bound to enable early warning while avoiding labels that are too temporally distant from the collision. The statistics of the collected dataset is shown in Table II.

Metrics. We evaluate monitoring effectiveness at both the scenario and frame levels using *Precision*, *Recall*, and *F1-score*. Precision measures the proportion of warnings that correctly indicate an impending collision, while Recall measures the proportion of impending collisions successfully detected. F1-score balances Precision and Recall, and FPR measures the proportion of safe instances incorrectly flagged as unsafe. Following prior work [8], we select two thresholds for each method on the validation set, targeting *False-Positive Rate (FPR)* of 0.01 and 0.05. We apply the selected thresholds unchanged to the test set and report the resulting Precision, Recall, and F1-score. We also report *AUROC* and *AUPRC* to assess discrimination performance across all possible thresholds.

Implementation Settings. We set the evolution budget T_{budget} to six hours, N_{round} to 20, and the temporal context length L to 5. Runtime signals are collected at 20 Hz, and the neighborhood radius δ is set to 20% of each parameter range. We implement *EvoEye* using PyTorch [31]. For a fair comparison, all evolution methods are given the same six-hour budget. All experiments are conducted on a Linux server equipped with an AMD EPYC 7543P CPU, an NVIDIA RTX A5000 GPU, and 256 GB of RAM.

A. RQ1: Monitoring Effectiveness

In this RQ, we compare the effectiveness of *EvoEye* with the baseline monitors. Table III shows both frame-level and scenario-level results. For the scenario-level, a violation is detected only when at least K consecutive frames are predicted as positive. We set $K = 1$ and $K = 3$ to evaluate both immediate detection and robustness to isolated false warnings. All methods (train and test) use the dataset shown in Table II.

1) *Frame-level effectiveness.*: *EvoEye* achieves the best frame-level performance on both scenarios and at both target FPRs. On S1, its F1-scores reach 30.1% and 29.1% at target FPRs of 0.05 and 0.01, respectively, compared with at most 7.5% and 2.1% for the baselines. On S2, *EvoEye* improves the corresponding F1-scores over the strongest baseline, TTC, from 41.6% to 67.8% and from 15.3% to 39.0%. It also achieves the highest AUROC and AUPRC on both scenarios, confirming that the improvement is not tied to a specific threshold. Overall, *EvoEye* better separates collision-preceding contexts from safe ones under controlled false-warning rates.

2) *Scenario-level effectiveness.*: The frame-level advantage of *EvoEye* translates into reliable scenario-level detection. With $K = 1$, *EvoEye* achieves the highest F1-score in all settings, reaching 54.3% and 55.3% on S1 and 87.9% and 76.6% on S2 at target FPRs of 0.05 and 0.01, respectively. When $K = 3$

Table III: Monitoring effectiveness on the two logical scenarios.

Method	S1: Highway Cut-in						S2: Unprotected Intersection						ROC↑	PRC↑		
	FPR = 0.05			FPR = 0.01			FPR = 0.05			FPR = 0.01						
	Prec.↑	Rec.↑	F1↑	Prec.↑	Rec.↑	F1↑	Prec.↑	Rec.↑	F1↑	Prec.↑	Rec.↑	F1↑				
Frame-level																
TTC	0.0	0.0	0.0	0.0	0.0	0.0	55.8	4.2	51.3	35.0	41.6	54.3	8.9	15.3	85.7	46.1
RSS	0.0	0.0	0.0	0.0	0.0	0.0	59.9	5.3	40.5	2.0	3.7	40.5	2.0	3.7	50.6	16.2
AEM	5.7	11.1	7.5	3.3	1.5	2.1	57.9	4.7	32.6	23.4	27.2	28.7	7.2	11.5	71.4	26.8
EvoEye*	21.7	48.9	30.1	34.8	25.0	29.1	77.4	21.9	71.1	64.8	67.8	86.3	25.2	39.0	91.8	71.8
Scenario-level ($K = 1$)																
TTC	0.0	0.0	0.0	0.0	0.0	0.0	39.9	28.9	75.0	100.0	85.7	71.8	74.7	73.3	43.0	72.2
RSS	30.0	12.0	17.1	30.0	12.0	17.1	49.1	34.0	80.0	32.3	46.0	80.0	32.3	46.0	54.1	78.7
AEM	32.4	96.0	48.5	23.2	52.0	32.1	26.2	24.4	71.9	82.8	77.0	79.4	50.5	61.7	51.1	74.9
EvoEye*	37.3	100.0	54.3	41.2	84.0	55.3	63.2	41.6	79.0	99.0	87.9	94.1	64.6	76.6	83.6	91.8
Scenario-level ($K = 3$)																
TTC	0.0	0.0	0.0	0.0	0.0	0.0	35.4	27.0	75.0	100.0	85.7	69.1	47.5	56.3	43.7	71.3
RSS	25.0	4.0	6.9	25.0	4.0	6.9	48.9	33.0	75.9	22.2	34.4	75.9	22.2	34.4	51.7	79.0
AEM	29.5	72.0	41.9	16.0	16.0	16.0	32.6	25.8	78.7	63.6	70.4	75.0	24.2	36.6	51.3	73.8
EvoEye*	39.1	100.0	56.2	45.7	64.0	53.3	69.2	50.7	83.5	91.9	87.5	96.5	55.6	70.5	83.4	91.8

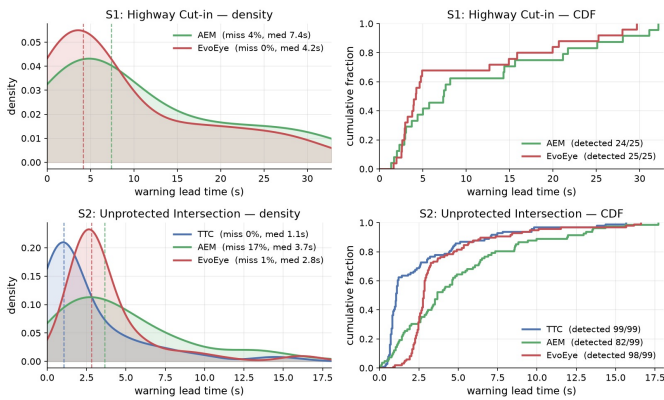


Fig. 3: Warning lead time distribution.

consecutive positive frames are required, *EvoEye* remains the best-performing method, with F1-scores of 56.2% and 53.3% on S1 and 87.5% and 70.5% on S2. It still detects all S1 violations and 91.9% of S2 violations at the 0.05 target FPR, indicating that its warnings persist across consecutive hazardous frames rather than arising from isolated predictions.

In contrast, the scenario-level Recall of some baselines is inflated by sporadic false warnings. With $K = 1$, any alerted frame can mark a violation scenario as detected, even when the alert occurs on a safe frame outside the prediction window. For example, RSS detects 3/25 S1 violations, although all alerted frames are safe, resulting in zero frame-level Recall. Together with its near-random AUROC, this suggests that RSS identifies violation scenarios largely through indiscriminate alerts. By contrast, the strong frame-level performance of *EvoEye* and its stability from $K = 1$ to $K = 3$ show that its scenario-level detections are supported by consistent responses to genuinely hazardous runtime contexts.

3) *Runtime Practicality*: Fig. 3 evaluates whether warnings are raised with sufficient lead time for intervention. Warning lead time is not necessarily better when longer, as excessively

early warnings may be triggered before the collision risk is sufficiently evident and thus increase false alarms. A practical monitor should therefore balance warning timeliness, detection coverage, and false-warning control. On S1, *EvoEye* detects all 25 violations with a median lead time of 4.2 seconds. On S2, it detects 98 of 99 violations with a median lead time of 2.8 seconds. In comparison, TTC detects all violations but warns only 1.1 seconds before collision, while AEM provides 3.7 seconds of warning but misses 17 violations. These results show that *EvoEye* provides near-complete detection with timely, rather than excessively early, warnings.

EvoEye also incurs low inference overhead. Processing one runtime context takes 2.49 ms on the CPU and 3.06 ms on the GPU, both well below the 50–100 ms ADS control cycle. The slightly lower CPU latency results from the small model size of approximately 25K parameters, for which GPU launch and data-transfer overheads dominate. Thus, *EvoEye* supports real-time deployment without dedicated GPU resources.

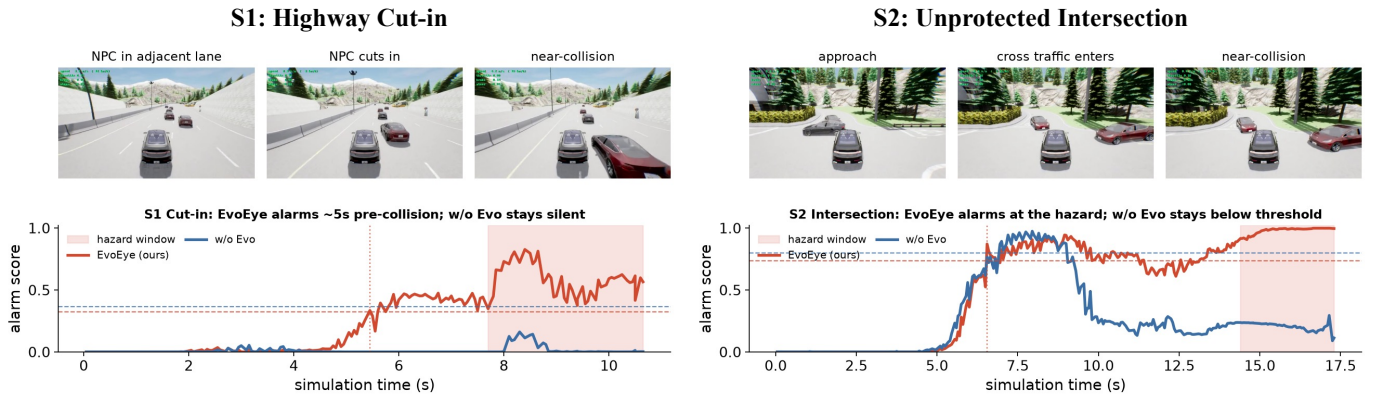
Answer to RQ1: The designed monitor in *EvoEye* provides the most effective and reliable monitoring, with timely warnings and millisecond-level inference overhead.

B. RQ2: Self-Evolution Effectiveness

1) *Comparative Results.*: Table IV evaluates whether self-evolution improves general monitoring performance and mitigates existing blind spots. The *Test Set* is the original test set summarized in Table II, while the *Hard Set* contains unsafe frames missed by *EvoEye** before evolution, together with the safe frames from the corresponding executions. As shown in Table IV, *EvoEye* achieves the highest F1, AUROC, and AUPRC across both scenarios and evaluation sets, outperforming Uniform and AVFuzzer under the same evolution budget. This indicates that monitor-oriented evolution is more effective than collecting additional data through unguided or safety-oriented search.

Table IV: Effectiveness of self-evolution (frame-level evaluation).

Method	<i>S1: Highway Cut-in</i>								<i>S2: Unprotected Intersection</i>							
	FPR = 0.05			FPR = 0.01			ROC↑	PRC↑	FPR = 0.05			FPR = 0.01			ROC↑	PRC↑
	Prec.↑	Rec.↑	F1↑	Prec.↑	Rec.↑	F1↑			Prec.↑	Rec.↑	F1↑	Prec.↑	Rec.↑	F1↑		
Test Set																
<i>EvoEye*</i>	21.7	48.9	30.1	34.8	25.0	29.1	77.4	21.9	71.1	64.8	67.8	86.3	25.2	39.0	91.8	71.8
<i>Uniform</i>	23.2	42.6	30.0	36.2	14.9	20.8	73.5	19.6	69.3	69.5	69.3	82.3	42.0	55.4	93.6	74.6
<i>AVFuzzer</i>	22.4	39.9	28.4	37.9	20.4	26.5	72.3	19.8	70.7	65.8	68.1	83.1	35.9	49.8	92.5	71.8
<i>EvoEye</i>	24.8	56.4	34.4	40.7	32.3	35.7	80.0	29.7	68.5	75.0	71.5	84.8	48.4	61.5	94.3	77.4
Hard Set																
<i>EvoEye*</i>	0.0	0.0	0.0	0.0	0.0	0.0	59.6	4.9	0.0	0.0	0.0	0.0	0.0	0.0	84.6	29.8
<i>Uniform</i>	10.6	13.5	11.7	29.8	8.0	12.4	59.4	5.9	47.8	38.8	42.7	75.8	28.0	40.6	89.8	41.8
<i>AVFuzzer</i>	9.5	12.9	10.8	21.6	9.3	12.5	58.1	4.7	48.7	30.2	37.2	76.0	22.6	34.2	87.0	38.9
<i>EvoEye</i>	17.3	31.2	22.2	36.0	20.4	25.7	69.4	13.5	49.4	47.9	48.4	80.7	35.6	49.1	90.9	49.5

Fig. 4: Illustrative cases comparing *EvoEye* before and after self-evolution.

On the *Test Set*, *EvoEye* consistently improves the initial monitor. Compared with *EvoEye**, *EvoEye* increases F1 from 30.1% to 34.4% on S1 and from 67.8% to 71.5% on S2 at the 0.05 target FPR. Under the stricter 0.01 target FPR, the corresponding gains are from 29.1% to 35.7% and from 39.0% to 61.5%. These improvements mainly result from higher Recall, indicating that evolution expands the monitor’s coverage while controlling false alarms.

The improvement is more evident on the *Hard Set*. Although *EvoEye** fails to detect these unsafe frames, *EvoEye* achieves F1-scores of 22.2% and 25.7% on S1 and 48.4% and 49.1% on S2 at the two target FPRs. It exceeds the strongest baseline by 10.5–13.2 F1 points on S1 and 5.7–8.5 points on S2, demonstrating that its evolution strategy more effectively acquires data that address the current monitor’s weaknesses.

Case Analysis. Fig. 4 shows that self-evolution enables *EvoEye* to produce stronger and more persistent responses to hazardous contexts. In S1, *EvoEye* raises an alarm approximately 5 seconds before the collision while *EvoEye** remains silent; in S2, *EvoEye* maintains its warning as the hazard develops, whereas *EvoEye** falls below the threshold.

Finding. Self-evolution improves both overall monitoring and blind-spot detection, outperforming both uniform and safety-oriented search under the same budget.

Table V: Ablation results for the monitor design on the Test Set at FPR 0.05.

Variant	<i>S1</i>			<i>S2</i>		
	F1↑	ROC↑	PRC↑	F1↑	ROC↑	PRC↑
<i>Temporal</i>						
$L = 1$	22.5	72.5	13.4	63.8	89.9	68.9
$L = 3$	29.0	73.0	20.4	65.5	91.4	68.4
$L = 5$	30.1	77.4	21.9	67.8	91.8	71.8
$L = 7$	28.5	74.3	21.3	65.2	91.5	68.0
<i>Inputs</i>						
Perc. only	28.3	71.9	18.4	62.0	90.5	66.0
Perc.+Pred.	28.9	73.2	17.2	60.8	90.0	64.1
Perc.+Pred.+Plan.	26.7	74.2	20.3	65.8	91.0	69.8
<i>EvoEye*</i>	30.1	77.4	21.9	67.8	91.8	71.8

C. RQ3: Component Contributions

In this section, we conduct ablation studies on the designs of both *FusionMonitor* and *BlindSpotEvolver*.

1) *Monitor Ablation:* Table V evaluates two key design choices of *FusionMonitor*: temporal context length and cross-module runtime inputs. We vary L while fixing the input signals, and progressively add module inputs while fixing $L = 5$.

Temporal context. Multi-frame contexts consistently outperform single-frame monitoring. Increasing L from 1 to 5 improves F1 by 7.6 points on S1 and 4.0 points on S2, with

Table VI: Ablation results for the self-evolution mechanisms on the Test Set at FPR 0.05.

Part	Variant	S1			S2		
		F1↑	ROC↑	PRC↑	F1↑	ROC↑	PRC↑
Comp.	<i>w/o Feedback</i>	30.6	79.5	24.0	68.2	92.5	74.1
	<i>w/o Density</i>	28.6	80.0	25.0	70.8	94.2	77.3
Monitor	<i>AEM</i>	7.5	57.9	4.7	27.2	71.4	26.8
	<i>AEM-Evo</i>	6.6	57.8	4.6	28.7	72.2	27.8
<i>EvoEye</i>	-	34.4	80.0	29.7	71.5	94.3	77.4

clear AUROC and AUPRC gains. The performance decrease at $L = 7$ indicates that longer histories may introduce noises.

Cross-module inputs. Using all runtime inputs achieves the highest performance on both scenarios. Compared with perception-only input, the complete model improves F1 by 1.8 points on S1 and 5.8 points on S2. The non-monotonic results of the intermediate variants further indicate that individual module signals are insufficient in isolation; their complementary information is most effective when jointly modeled.

Overall, the results confirm that both temporal context modeling and cross-module fusion contribute to the *FusionMonitor*.

2) *Self-Evolution:* Table VI evaluates the contributions of *Monitor-Oriented Feedback*, *Density-Aware Mutation*, and the *underlying monitor*. As shown in Table VI, we find that removing feedback decreases F1 by 3.8 points on S1 and 3.3 points on S2, confirming that prediction errors effectively guide the acquisition of scenarios that expose current monitoring weaknesses. Removing density awareness causes the largest F1 drop on S1 (5.8 points) and a smaller drop on S2 (0.7 points), showing its benefit in adaptive mutation. Finally, applying evolution to AEM yields no improvement on S1 and only a 1.5-point F1 gain on S2. This indicates that effective self-evolution requires both informative scenario acquisition and a monitor capable of learning from the acquired records.

Answer to RQ3: Temporal and cross-module modeling improve monitoring, while effective self-evolution depends on feedback, density awareness, and monitor learning capacity.

D. Threats to Validity

(1) *Internal Threats.* The stochasticity of scenario evolution may affect the collected executions and the resulting monitor performance. To mitigate this threat, we repeat each evolution experiment three times and use the same initial dataset, evolution budget, and test set for all compared methods. Another threat lies in the choice of prediction horizon H , which determines the frame-level labels. We set $H = 3$ seconds based on prior studies [9], [29], [30] of pre-crash intervention. (2) *External Threats.* Our evaluation is conducted on Baidu Apollo with CARLA and covers two logical scenarios, which may limit generalization to other ADSs and driving conditions. Nevertheless, *EvoEye* is not tied to a specific ADS architecture, although its runtime-signal extractors must be adapted to different module interfaces. Moreover, simulation cannot fully reproduce real-world sensing and traffic conditions.

We mitigate this threat by retaining Apollo’s complete sensor-to-control pipeline rather than providing simulator ground truth directly to the ADS. Finally, we focus on collisions; extending *EvoEye* to other safety violations remains future work.

VI. RELATED WORK

Runtime Monitoring for ADS. Runtime monitoring aims to detect abnormal or safety-critical behaviors that arise during the operation of autonomous driving systems (ADSs). Existing approaches broadly fall into two categories: rule-based and learning-based monitoring. Rule-based monitors assess runtime safety using predefined safety indicators or formal specifications, such as Time-to-Collision (TTC) [6] and Responsibility-Sensitive Safety (RSS) [7]. These approaches are typically efficient, interpretable, and easy to deploy. However, predefined rules and limited kinematic variables restrict these monitors to known conflict patterns, making them less effective for complex ADS failures. Learning-based monitors instead learn indicators of unsafe behavior from runtime data. For example, SelfOracle [8] detects ADS misbehavior based on the reconstruction errors of sensor inputs, whereas Third-Eye [9] leverages attention maps to predict impending failures. Although these approaches can capture failure patterns that are difficult to specify manually, they predominantly rely on observations tied to individual components. Such observations provide only a partial view of a full-stack ADS, whose runtime behavior emerges from the interactions among different modules. In contrast, *EvoEye* jointly monitors internal runtime signals across multiple modules to characterize the system-level behavior of a full-stack ADS.

Scenario Search for ADS. The large and continuous scenario space of ADSs makes exhaustive exploration infeasible. Search-based testing has therefore become a mainstream approach for identifying safety-critical scenarios [22], [23], [25], [27], [32]–[40]. Existing techniques include guided fuzzing [23], [25], [41]–[44], evolutionary search [32], [34]–[37], [39], [45], [46], metamorphic testing [47], surrogate model-guided search [22], [33], [48], and reinforcement learning [26], [49], [50]. These approaches primarily optimize for exposing safety violations and evaluating the ADS under test. However, scenarios that are effective for ADS testing may provide limited value for runtime monitor improvement, particularly when the corresponding failures can already be detected. In this paper, we address this limitation by using feedback from the current monitor to guide scenario search, prioritizing scenarios that expose its detection weaknesses and incorporating them into subsequent updates.

VII. CONCLUSION

In this paper, we present *EvoEye*, a self-evolving runtime monitoring approach for autonomous driving systems. *EvoEye* integrates two key components: *FusionMonitor*, which learns from heterogeneous and temporally dependent runtime signals to predict impending collisions, and *BlindSpotEvolver*, which uses *Monitor-Oriented Feedback* and *Density-Aware Mutation* to iteratively acquire informative scenario records and improve

the monitor within a limited budget. Our evaluation demonstrates that *EvoEye* provides effective and timely collision warnings, incurs low runtime overhead, and progressively improves its monitoring capability through self-evolution. Results also show the contribution of each component.

VIII. ACKNOWLEDGEMENT

This research is partially supported by the Ministry of Education, Singapore under its Academic Research Fund Tier 2 (Proposal ID: T2EP20223-0043; Project ID: MOE-000613-00). Any opinions, findings and conclusions or recommendations expressed in this material are those of the author(s) and do not reflect the views of the Ministry of Education, Singapore. Lionel Briand was funded by Research Ireland under Grant number 13/RC/2094 2 and the Natural Sciences and Engineering Research Council of Canada.

REFERENCES

- [1] B. Paden, M. Čáp, S. Z. Yong, D. Yershov, and E. Frazzoli, "A survey of motion planning and control techniques for self-driving urban vehicles," *IEEE Transactions on intelligent vehicles*, vol. 1, no. 1, pp. 33–55, 2016.
- [2] C. Badue, R. Guidolini, R. V. Carneiro, P. Azevedo, V. B. Cardoso, A. Forechi, L. Jesus, R. Berriel, T. M. Paixao, F. Mutz *et al.*, "Self-driving cars: A survey," *Expert systems with applications*, vol. 165, p. 113816, 2021.
- [3] P. Koopman and M. Wagner, "Challenges in autonomous vehicle testing and validation," *SAE International journal of transportation safety*, vol. 4, pp. 15–24, 2016.
- [4] G. Lou, Y. Deng, X. Zheng, M. Zhang, and T. Zhang, "Testing of autonomous driving systems: where are we and where should we go?" in *Proceedings of the 30th ACM Joint European Software Engineering Conference and Symposium on the Foundations of Software Engineering*, 2022, pp. 31–43.
- [5] K. Watanabe, E. Kang, C.-W. Lin, and S. Shiraishi, "Runtime monitoring for safety of intelligent vehicles," in *Proceedings of the 55th annual design automation conference*, 2018, pp. 1–6.
- [6] J. C. Hayward, "Near miss determination through use of a scale of danger," *Highway Research Record*, 1972.
- [7] S. Shalev-Shwartz, S. Shammah, and A. Shashua, "On a formal model of safe and scalable self-driving cars," *arXiv preprint arXiv:1708.06374*, 2017.
- [8] A. Stocco, M. Weiss, M. Calzana, and P. Tonella, "Misbehaviour prediction for autonomous driving systems," in *Proceedings of the ACM/IEEE 42nd international conference on software engineering*, 2020, pp. 359–371.
- [9] A. Stocco, P. J. Nunes, M. d'Amorim, and P. Tonella, "Thirdeye: Attention maps for safe autonomous driving systems," in *Proceedings of the 37th IEEE/ACM international conference on automated software engineering*, 2022, pp. 1–12.
- [10] Baidu, "Baidu-apollo," 2023. [Online]. Available: <https://www.apollo.auto>
- [11] A. Dosovitskiy, G. Ros, F. Codevilla, A. Lopez, and V. Koltun, "Carla: An open urban driving simulator," in *Conference on robot learning*. PMLR, 2017, pp. 1–16.
- [12] I. Gog, S. Kalra, P. Schafhalter, M. A. Wright, J. E. Gonzalez, and I. Stoica, "Pylot: A modular platform for exploring latency-accuracy tradeoffs in autonomous vehicles," in *2021 IEEE International Conference on Robotics and Automation (ICRA)*. IEEE, 2021, pp. 8806–8813.
- [13] S. Kato, S. Tokunaga, Y. Maruyama, S. Maeda, M. Hirabayashi, Y. Kitsukawa, A. Monroy, T. Ando, Y. Fujii, and T. Azumi, "Autoware on board: Enabling autonomous vehicles with embedded systems," in *2018 ACM/IEEE 9th International Conference on Cyber-Physical Systems (ICPPS)*. IEEE, 2018, pp. 287–296.
- [14] M. Bojarski, D. Del Testa, D. Dworakowski, B. Firner, B. Flepp, P. Goyal, L. D. Jackel, M. Monfort, U. Muller, J. Zhang *et al.*, "End to end learning for self-driving cars," *arXiv preprint arXiv:1604.07316*, 2016.
- [15] F. Codevilla, M. Müller, A. López, V. Koltun, and A. Dosovitskiy, "End-to-end driving via conditional imitation learning," in *2018 IEEE international conference on robotics and automation (ICRA)*. IEEE, 2018, pp. 4693–4700.
- [16] comma.ai, "openpilot," 2025. [Online]. Available: <https://comma.ai/openpilot>
- [17] Z. Zhang, A. Liniger, D. Dai, F. Yu, and L. Van Gool, "End-to-end urban driving by imitating a reinforcement learning coach," in *Proceedings of the IEEE/CVF international conference on computer vision*, 2021, pp. 15 222–15 232.
- [18] K. Chitta, A. Prakash, B. Jaeger, Z. Yu, K. Renz, and A. Geiger, "Transfuser: Imitation with transformer-based sensor fusion for autonomous driving," *IEEE Transactions on Pattern Analysis and Machine Intelligence*, vol. 45, no. 11, pp. 12 878–12 895, 2023.
- [19] P. Wu, X. Jia, L. Chen, J. Yan, H. Li, and Y. Qiao, "Trajectory-guided control prediction for end-to-end autonomous driving: A simple yet strong baseline," *Advances in Neural Information Processing Systems*, vol. 35, pp. 6119–6132, 2022.
- [20] E. Thorn, S. C. Kimmel, and M. Chaka, "A framework for automated driving system testable cases and scenarios," National Highway Traffic Safety Administration, Tech. Rep., 2018.
- [21] T. Menzel, G. Bagnschik, and M. Maurer, "Scenarios for development, test and validation of automated vehicles," in *2018 IEEE intelligent vehicles symposium (IV)*. IEEE, 2018, pp. 1821–1827.
- [22] F. U. Haq, D. Shin, and L. Briand, "Efficient online testing for dnn-enabled systems using surrogate-assisted and many-objective optimization," in *Proceedings of the 44th international conference on software engineering*, 2022, pp. 811–822.
- [23] G. Li, Y. Li, S. Jha, T. Tsai, M. Sullivan, S. K. S. Hari, Z. Kalbarczyk, and R. Iyer, "Av-fuzzer: Finding safety violations in autonomous driving systems," in *2020 IEEE 31st international symposium on software reliability engineering (ISSRE)*. IEEE, 2020, pp. 25–36.
- [24] S. Sharifi, D. Shin, L. C. Briand, and N. Aschbacher, "Identifying the hazard boundary of ml-enabled autonomous systems using cooperative coevolutionary search," *IEEE Transactions on Software Engineering*, vol. 49, no. 12, pp. 5120–5138, 2023.
- [25] M. Cheng, Y. Zhou, and X. Xie, "Behavexplor: Behavior diversity guided testing for autonomous driving systems," in *Proceedings of the 32nd ACM SIGSOFT International Symposium on Software Testing and Analysis*, 2023, pp. 488–500.
- [26] F. U. Haq, D. Shin, and L. C. Briand, "Many-objective reinforcement learning for online testing of dnn-enabled systems," in *2023 IEEE/ACM 45th International Conference on Software Engineering (ICSE)*. IEEE, 2023, pp. 1814–1826.
- [27] Y. Huai, Y. Chen, S. Almanee, T. Ngo, X. Liao, Z. Wan, Q. A. Chen, and J. Garcia, "Doppelgänger test generation for revealing bugs in autonomous driving software," in *2023 IEEE/ACM 45th International Conference on Software Engineering (ICSE)*. IEEE, 2023, pp. 2591–2603.
- [28] W. G. Najm, J. D. Smith, and M. Yanagisawa, "Pre-crash scenario typology for crash avoidance research," U.S. Department of Transportation National Highway Traffic Safety Administration, Tech. Rep., 2007.
- [29] J. K. Lee and K. W. Lee, "Study on effectiveness of pre-crash active seatbelt using real time controlled simulation," in *23rd International Technical Conference on the Enhanced Safety of Vehicles (ESV) National Highway Traffic Safety Administration*, no. 13-0097, 2013.
- [30] Z. Zhao, L. Zhou, Q. Zhu, Y. Luo, and K. Li, "A review of essential technologies for collision avoidance assistance systems," *Advances in Mechanical Engineering*, vol. 9, no. 10, p. 1687814017725246, 2017.
- [31] A. Paszke, S. Gross, F. Massa, A. Lerer, J. Bradbury, G. Chanan, T. Killeen, Z. Lin, N. Gimelshein, L. Antiga *et al.*, "Pytorch: An imperative style, high-performance deep learning library," *Advances in neural information processing systems*, vol. 32, 2019.
- [32] S. Han, J. Kim, G. Kim, J. Cho, J. Kim, and S. Yoo, "Preliminary evaluation of path-aware crossover operators for search-based test data generation for autonomous driving," in *2021 IEEE/ACM 14th International Workshop on Search-Based Software Testing (SBST)*. IEEE, 2021, pp. 44–47.
- [33] Z. Zhong, G. Kaiser, and B. Ray, "Neural network guided evolutionary fuzzing for finding traffic violations of autonomous vehicles," *IEEE Transactions on Software Engineering*, vol. 49, no. 4, pp. 1860–1875, 2023.
- [34] Y. Tang, Y. Zhou, T. Zhang, F. Wu, Y. Liu, and G. Wang, "Systematic testing of autonomous driving systems using map topology-based scenario classification," in *2021 36th IEEE/ACM International Conference on Automated Software Engineering (ASE)*. IEEE, 2021, pp. 1342–1346.
- [35] Y. Zhou, Y. Sun, Y. Tang, Y. Chen, J. Sun, C. M. Poskitt, Y. Liu, and Z. Yang, "Specification-based autonomous driving system testing," *IEEE*

Transactions on Software Engineering, vol. 49, no. 6, pp. 3391–3410, 2023.

- [36] Y. Tang, Y. Zhou, F. Wu, Y. Liu, J. Sun, W. Huang, and G. Wang, “Route coverage testing for autonomous vehicles via map modeling,” in *2021 IEEE International Conference on Robotics and Automation (ICRA)*. IEEE, 2021, pp. 11 450–11 456.
- [37] Y. Tang, Y. Zhou, Y. Liu, J. Sun, and G. Wang, “Collision avoidance testing for autonomous driving systems on complete maps,” in *2021 IEEE Intelligent Vehicles Symposium (IV)*. IEEE, 2021, pp. 179–185.
- [38] R. Wang, M. Cheng, X. Xie, Y. Zhou, and L. Ma, “Moditector: Module-directed testing for autonomous driving systems,” *Proceedings of the ACM on Software Engineering*, vol. 2, no. ISSTA, pp. 137–158, 2025.
- [39] H. Yousefzadeh, S. Gu, L. C. Briand, and A. Nasr, “Using cooperative co-evolutionary search to generate metamorphic test cases for autonomous driving systems,” *IEEE Transactions on Software Engineering*, 2025.
- [40] M. Cheng, L. Briand, and Y. Zhou, “Drivora: A unified and extensible infrastructure for search-based autonomous driving testing,” *arXiv preprint arXiv:2601.05685*, 2026.
- [41] Q. Pang, Y. Yuan, and S. Wang, “Mdpfuzz: testing models solving markov decision processes,” in *Proceedings of the 31st ACM SIGSOFT International Symposium on Software Testing and Analysis*, 2022, pp. 378–390.
- [42] M. Cheng, R. Wang, X. Xie, Y. Zhou, and L. Ma, “Stclocker: Deadlock avoidance testing for autonomous driving systems,” *arXiv preprint arXiv:2506.23995*, 2025.
- [43] W. Tang, M. Cheng, R. Wang, Y. Zhou, C. Liu, Y. Liu, and Z. Ding, “Causality-aware safety testing for autonomous driving systems,” *IEEE Transactions on Software Engineering*, 2026.
- [44] M. Cheng, X. Xie, Y. Zhou, J. Wang, G. Meng, and K. Yang, “Decictor: Towards evaluating the robustness of decision-making in autonomous driving systems,” in *2025 IEEE/ACM 47th International Conference on Software Engineering (ICSE)*. IEEE, 2025, pp. 1–13.
- [45] A. Gambi, M. Mueller, and G. Fraser, “Automatically testing self-driving cars with search-based procedural content generation,” in *Proceedings of the 28th ACM SIGSOFT International Symposium on Software Testing and Analysis*, 2019, pp. 318–328.
- [46] H. Yousefzadeh, S. Gu, L. C. Briand, and A. Nasr, “Constrained co-evolutionary metamorphic differential testing for autonomous systems with an interpretability approach,” *arXiv preprint arXiv:2509.16478*, 2025.
- [47] J. C. Han and Z. Q. Zhou, “Metamorphic fuzz testing of autonomous vehicles,” in *Proceedings of the IEEE/ACM 42nd International Conference on Software Engineering Workshops*, 2020, pp. 380–385.
- [48] Z. Li, X. Wu, D. Zhu, M. Cheng, S. Chen, F. Zhang, X. Xie, L. Ma, and J. Zhao, “Generative model-based testing on decision-making policies,” in *2023 38th IEEE/ACM International Conference on Automated Software Engineering (ASE)*. IEEE, 2023, pp. 243–254.
- [49] S. Feng, H. Sun, X. Yan, H. Zhu, Z. Zou, S. Shen, and H. X. Liu, “Dense reinforcement learning for safety validation of autonomous vehicles,” *Nature*, vol. 615, no. 7953, pp. 620–627, 2023.
- [50] C. Lu, Y. Shi, H. Zhang, M. Zhang, T. Wang, T. Yue, and S. Ali, “Learning configurations of operating environment of autonomous vehicles to maximize their collisions,” *IEEE Transactions on Software Engineering*, vol. 49, no. 1, pp. 384–402, 2023.